

# Automatic Detection and Segmentation of Evolving Processes in 3D Medical Images: Application to Multiple Sclerosis

David Rey, Gérard Subsol, Hervé Delingette, Nicholas Ayache

## ► To cite this version:

David Rey, Gérard Subsol, Hervé Delingette, Nicholas Ayache. Automatic Detection and Segmentation of Evolving Processes in 3D Medical Images: Application to Multiple Sclerosis. RR-3559, INRIA. 1998. inria-00073125

**HAL Id: inria-00073125**

**<https://hal.inria.fr/inria-00073125>**

Submitted on 24 May 2006

**HAL** is a multi-disciplinary open access archive for the deposit and dissemination of scientific research documents, whether they are published or not. The documents may come from teaching and research institutions in France or abroad, or from public or private research centers.

L'archive ouverte pluridisciplinaire **HAL**, est destinée au dépôt et à la diffusion de documents scientifiques de niveau recherche, publiés ou non, émanant des établissements d'enseignement et de recherche français ou étrangers, des laboratoires publics ou privés.

***Automatic Detection and Segmentation of Evolving  
Processes in 3D Medical Images: Application to  
Multiple Sclerosis***

David Rey — Gérard Subsol — Hervé Delingette — Nicholas Ayache

**N° 3559**

November 1998

\_\_\_\_\_ THÈME 3 \_\_\_\_\_



***apport  
de recherche***





# Automatic Detection and Segmentation of Evolving Processes in 3D Medical Images: Application to Multiple Sclerosis

David Rey, Gérard Subsol, Hervé Delingette, Nicholas Ayache

Thème 3 — Interaction homme-machine,  
images, données, connaissances  
Projet Epidaure

Rapport de recherche n° 3559 — November 1998 — 19 pages

**Abstract:** Physicians often perform diagnoses based on the evolution of lesions, tumors or anatomical structures through time. The objective of this report is to automatically detect regions with apparent local volume variation with a vector field operator applied to the local displacement field obtained after a non-rigid registration between successive temporal images.

In studying the information of apparent shrinking areas in the direct and reverse displacement fields between images, we are able to segment evolving lesions. Then we propose a method to segment lesions in a whole temporal series of images.

In this report we apply this approach to the automatic detection and segmentation of multiple sclerosis lesions in time series of MRI images of the brain.

**Key-words:** 3D medical imaging, automatic detection and segmentation, evolving processes, vector field analysis, vector field operator, multiple sclerosis.

# Détection et segmentation automatiques de processus évolutifs dans des images médicales tridimensionnelles : application à la sclérose en plaques

**Résumé :** Les docteurs réalisent souvent des diagnostics en se fondant sur l'évolution de lésions, de tumeurs, ou de structures anatomiques au cours du temps. L'objectif de ce rapport est de proposer une méthode de détection automatique des régions où il y a une variation locale de volume apparente, grâce à un opérateur appliqué au champ de déplacements obtenu après une transformation non-rigide entre deux images temporelles successives.

En étudiant les informations fournies par les régions de décroissance apparentes dans les champs directs et réciproques entre deux images, nous sommes capables de segmenter les lésions évolutives. Nous proposons ensuite une méthode pour segmenter les lésions dans une série temporelle complète d'images.

Dans ce rapport nous appliquons cette approche pour la détection et la segmentation automatique des lésions de sclérose en plaques dans des séries temporelles d'images IRM du cerveau.

**Mots-clés :** imagerie médicale 3D, détection et segmentation automatique, processus évolutifs, analyse de champ de vecteurs, opérateur sur champ de vecteurs, sclérose en plaques.

# Contents

<b>1</b>	<b>Presentation of the problem</b>	<b>4</b>
1.1	Multiple sclerosis data . . . . .	4
1.2	Quantitative measurements . . . . .	4
1.3	A new method based on the displacement field . . . . .	6
<b>2</b>	<b>Computation of the displacement field</b>	<b>6</b>
2.1	Rigid registration . . . . .	6
2.2	Non-rigid registration . . . . .	7
<b>3</b>	<b>Vector field operators</b>	<b>9</b>
3.1	Principle . . . . .	9
3.2	The Jacobian operator . . . . .	9
3.2.1	Mathematical expression and physical meaning . . . . .	9
3.2.2	Robustness of the Jacobian with respect to misalignment . . . . .	10
3.2.3	Computation and application of the Jacobian . . . . .	10
3.3	Other operators . . . . .	10
<b>4</b>	<b>Thresholding and segmentation</b>	<b>12</b>
4.1	Method and results . . . . .	12
4.2	Time series segmentation . . . . .	12
<b>5</b>	<b>Robustness with respect to rigid alignment</b>	<b>13</b>
<b>6</b>	<b>Conclusion</b>	<b>13</b>

# 1 Presentation of the problem

## 1.1 Multiple sclerosis data

Multiple sclerosis is a progressive disease that requires an evolution study through time. The evolution of the disease can be followed on a patient with a temporal series of examinations. A time series of 3D images of a patient is acquired from the same modality and with a definite protocol to have similar properties: similar histogram, field of view, voxel size, image size, etc. In this report we use two sets of multiple sclerosis time series composed of T2 weighted MRI images. These two time series come from the Brigham and Women's Hospital <sup>1</sup> and from the BIOMORPH <sup>2</sup> European project. The data from the Brigham and Women's Hospital consist in  $256 \times 256 \times 54$  images, with a voxel size of  $0.9 \times 0.9 \times 3.0$  mm. The temporal interval between two images of the series is about one week. The data from the BIOMORPH project consist in  $256 \times 256 \times 24$  images with a voxel size of  $0.9 \times 0.9 \times 5.0$  mm. The temporal interval between two images of the series is about four weeks.

## 1.2 Quantitative measurements

A quantitative analysis is required to give accurate and reproducible results, and because the data are large. Between two examinations, a patient does not have the same position in the acquisition device. Therefore images at different times are not directly comparable. (cf Figure 1). We have to apply a transformation to

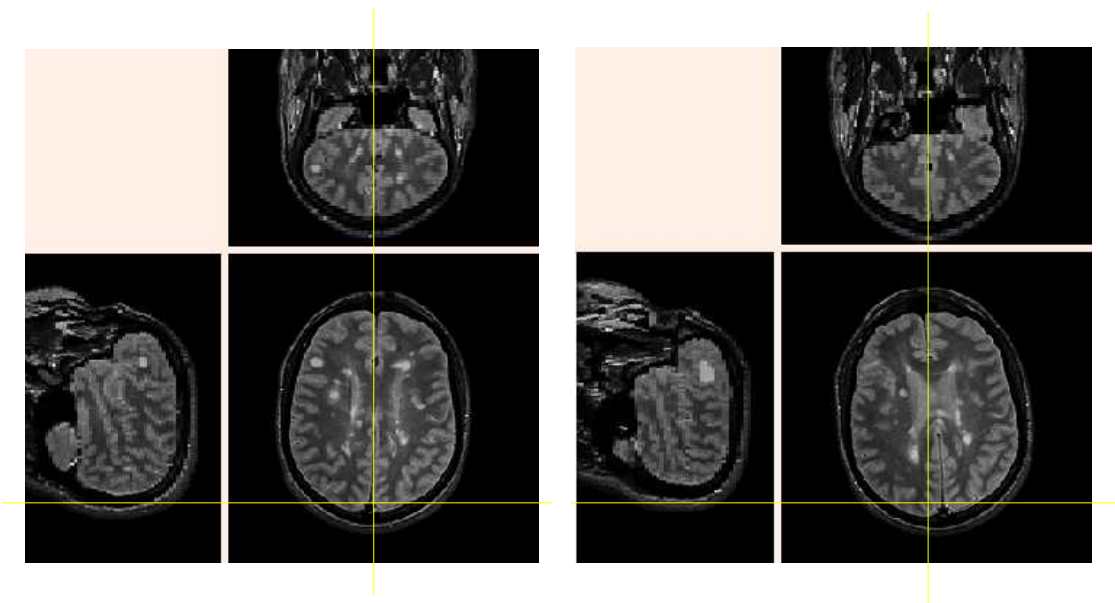


Figure 1: *Two images of a patient at different times. The voxels are not directly comparable.*

each image to compensate for the difference in position (translation) and orientation (rotation). Then we can compare the two images, and apply automatic computerized tools to detect and quantify evolving processes (cf Figure 2). There are several existing automatic methods to study the lesions of multiple sclerosis in time series:

- With a single image, it is possible to threshold or to study the image intensity to segment lesions [ZFE98]. Unfortunately, thresholding does not always make it possible to distinguish the lesions from the white matter.
- It is possible to subtract two successive images to find areas where the lesions have changed. But this method has two major problems. First, the subtraction is extremely dependent on the rigid registration [HSO<sup>+</sup>95], [Lem97]. For instance, we show in Figure 3 an evolving lesion that appears in the image of the subtraction as a dark hole. But when the registration is inaccurate, it is hard to distinguish evolving lesions: the edges of the anatomical structures appear (cortex, ventricles, etc.) and give the same apparent information as the lesions. Secondly, the subtraction only characterizes the difference of intensity between

<sup>1</sup>D<sup>r</sup> Guttman and D<sup>r</sup> Kikinis

<sup>2</sup><http://www.vision.ee.ethz.ch/~mastyner/biomorph/biomorph.html>

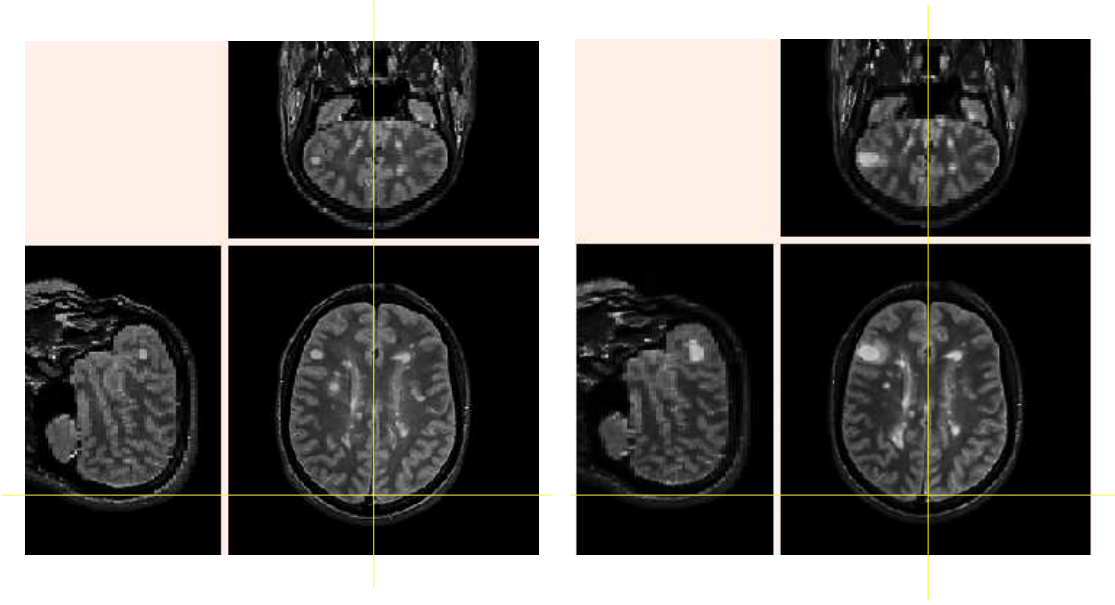


Figure 2: *Two images of a patient at different times have been registered. The voxels are now comparable.*

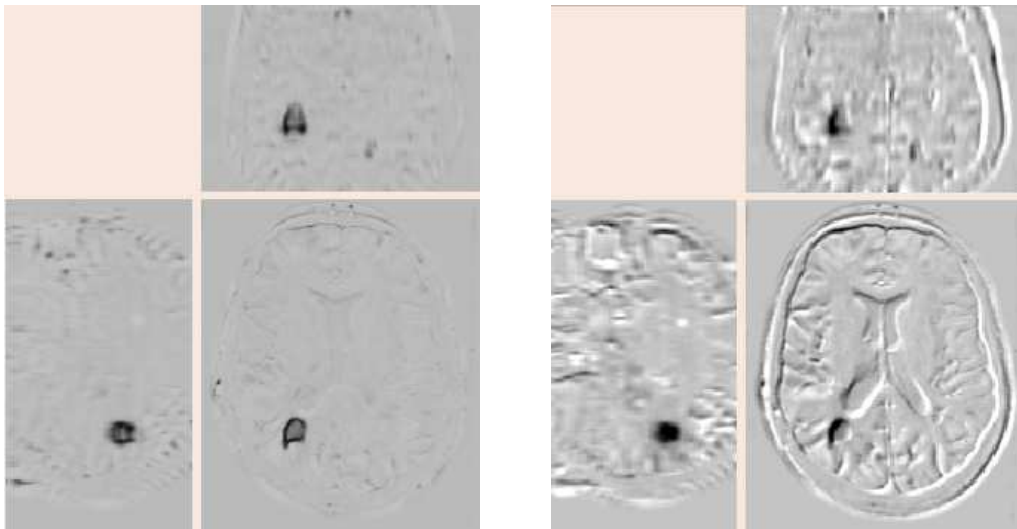


Figure 3: *Comparison between two subtractions with respect to the rigid registration. Left: correct rigid registration: it is easy to detect lesions that evolve (e.g. black hole for a shrinking lesion). Right: approximative rigid registration: all the anatomical structures appear (e.g. the ventricles, the edges of the brain) and it becomes very hard to distinguish lesions.*



two images. The image of the subtraction does not give a contrasted image with respect to the evolution ratio, but only with respect to the difference between the intensity of the lesion and the intensity of the background. For example we show in Figure 4 that if we threshold the image of the subtraction, only some parts of the evolving structures are detected. Moreover the threshold value is not related to the amplitude of the evolutions as can be seen in Figure 4 where a series of threshold values is applied to a synthesis example.

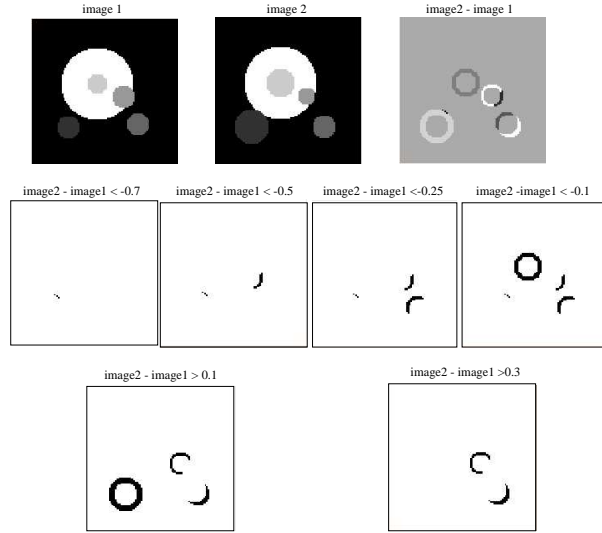


Figure 4: *Different threshold values applied to an image of subtraction. For each value, only some parts of the evolving structures are detected. Moreover, the threshold value is not related to the amplitude of the evolutions.*

- With  $n$  images, it is possible to follow the intensity of each voxel in time [GWG<sup>+</sup>98]. Although very nice results are obtained with perfectly rigidly aligned, the approach remains sensitive to the rigid registration, and there is no direct relation between the amplitude of evolution and the variation of voxels intensity. Moreover, this method does not take into account the spatial correlation between neighbouring voxels.

### 1.3 A new method based on the displacement field

Our idea is thus to avoid a voxel by voxel comparison and to use the “apparent” motion between two images. Figure 5 shows the different stages of the automatic processing and gives an overview of this report. First, images are aligned by a rigid registration. Then we compute the displacement field to recover the “apparent” motion between images with a non-rigid registration algorithm. We focus on the detection of the regions of interest of the field thanks to vector field operators, and use them to segment evolving lesions. This work is a natural continuation of the previous research work of Thirion and Calmon [TC97b].

## 2 Computation of the displacement field

### 2.1 Rigid registration

First we compute a rigid registration with an algorithm which matches “extremal” points defined as the maxima of the crest lines of the images [Thi96]. Feature points called “extremal” points are automatically extracted from the 3D image. They are defined as the loci of curvature extrema along the “crest lines” of the isosurface corresponding to the zero-crossing of the Laplacian of the image. Based on those stable points, a two-step registration algorithm computes a rigid transformation. The first step called “prediction” looks for triplets of points from the two sets which can be put into correspondence with respect to their invariant attributes. The second step called “verification” checks whether the 3D rigid transformation computed from the two corresponding triplets is valid for all the other points. A study of the accuracy of this algorithm, especially for aligning MS data, can be found in [PT97].

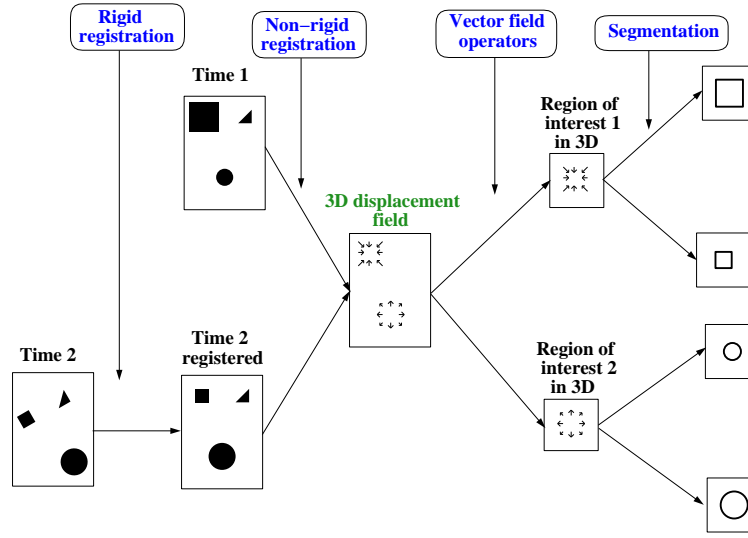


Figure 5: Method of detection and segmentation of evolving processes using the displacement field.

## 2.2 Non-rigid registration

We compute the 3D displacement field with a non-rigid algorithm based on local diffusion [Thi98]. This algorithm diffuses the first image into the second one. Each point of the second image “attracts” or “repels” the point that has the same coordinates with the first image according to their difference of intensity. All these forces are regularized and deform the second image. The process is iterated based on a multi-scale scheme. At the end, each point  $P(x, y, z)$  of the reference image has a vector  $\mathbf{u}(u_1, u_2, u_3)$  that gives its apparent **displacement** (cf Figure 7). As we can see in Figure 6, We can also defined the **deformation** which is a function  $\phi(\phi_1, \phi_2, \phi_3)$  that transforms the point  $P(x, y, z)$  in the point  $P'(x', y', z')$ . We can see in Figure 6 the deformation function and the displacement field between two images.

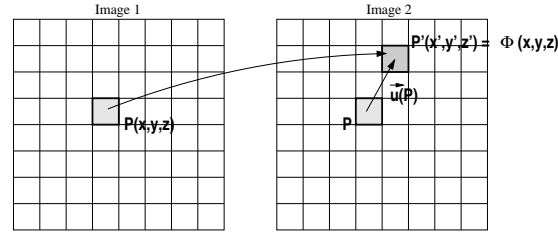


Figure 6: Definition of the displacement  $\mathbf{u}$  and the deformation  $\phi$  of a point  $P$ .

We have thus:

$$\begin{cases} x' &= x + u_1(x, y, z) = \phi_1(x, y, z) \\ y' &= y + u_2(x, y, z) = \phi_2(x, y, z) \\ z' &= z + u_3(x, y, z) = \phi_3(x, y, z) \end{cases}$$

This apparent displacement field  $\mathbf{u}$  gives an idea of the time evolution between two images. We can compute the two fields: from image 1 to image 2, and from image 2 to image 1, which contain complementary information as we will see in section 4.1. Figure 7 shows the vector field from 1 to 2 around a lesion, emphasizing a radial shrinking. Figure 8 shows the effect of the vector field from 2 to 1 on a regular grid on the global image, and on a region around two evolving lesions. We can see the effect of a shrinking and of an expansion on the grid.

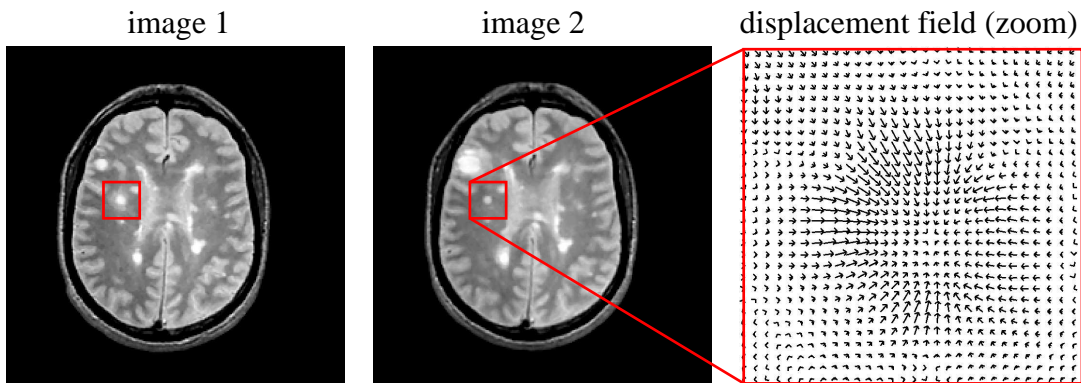


Figure 7: An example of the computation of the “apparent” displacement field thanks to a non-rigid registration algorithm. Notice how it emphasizes the shrinking lesion.

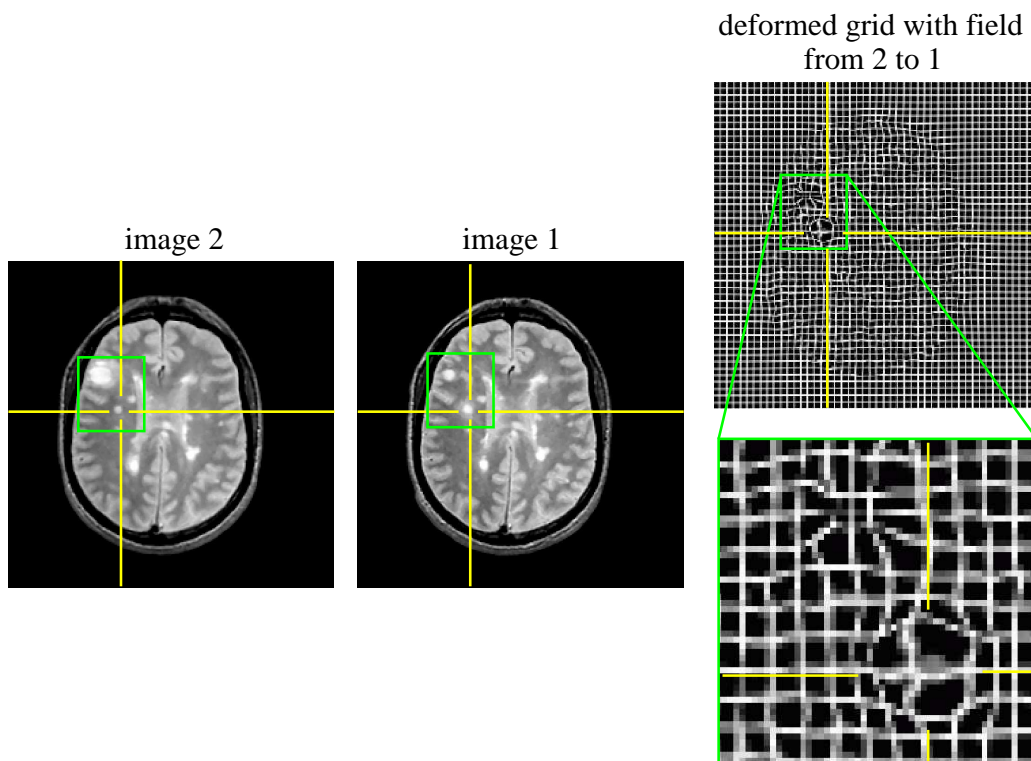


Figure 8: Application of the displacement field on a 3D grid.

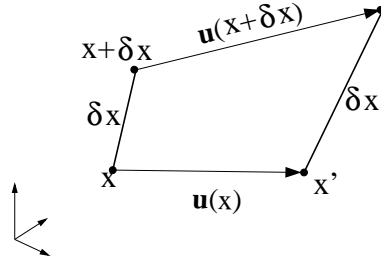


Figure 9: The point  $x$  at time 1 is coupled with a 3D vector of apparent displacement  $\mathbf{u}(x)$  that gives the point  $x'$  at time 2. Let us compute the length variation through time of the couple of points  $(x, \delta x)$  that are very close.

### 3 Vector field operators

#### 3.1 Principle

The vector field operators should transform a 3D vector field in a simpler representation that is a 3D scalar image. This scalar image should be contrasted with respect to the time evolutions. Moreover we need to introduce operators that have a physical meaning for a better interpretation.

#### 3.2 The Jacobian operator

##### 3.2.1 Mathematical expression and physical meaning

We introduce as an operator the Jacobian of the deformation function,  $\phi(\phi_1, \phi_2, \phi_3)$ , as inspired from [DVR<sup>+</sup>96]. This operator is widely used in continuum mechanics [BN97] [WMG97]. The Jacobian of  $\phi$  at point P is defined as:

$$Jacobian = \det(\nabla_p \phi) = \det \begin{pmatrix} \frac{\partial \phi_1}{\partial x} & \frac{\partial \phi_1}{\partial y} & \frac{\partial \phi_1}{\partial z} \\ \frac{\partial \phi_2}{\partial x} & \frac{\partial \phi_2}{\partial y} & \frac{\partial \phi_2}{\partial z} \\ \frac{\partial \phi_3}{\partial x} & \frac{\partial \phi_3}{\partial y} & \frac{\partial \phi_3}{\partial z} \end{pmatrix}$$

It can also be written with the vector displacement field  $\mathbf{u}(u_1, u_2, u_3)$  at P:

$$\det(\nabla_p \phi) = \det(Id + \nabla_p \mathbf{u}) = \det \begin{pmatrix} \frac{\partial u_1}{\partial x} + 1 & \frac{\partial u_1}{\partial y} & \frac{\partial u_1}{\partial z} \\ \frac{\partial u_2}{\partial x} & \frac{\partial u_2}{\partial y} + 1 & \frac{\partial u_2}{\partial z} \\ \frac{\partial u_3}{\partial x} & \frac{\partial u_3}{\partial y} & \frac{\partial u_3}{\partial z} + 1 \end{pmatrix}$$

It is useful to recall a physical interpretation of the Jacobian operator in terms of local variation of volume. With the notation of the Figure 9, each point  $x$  at time 1 is coupled with a 3D vector of apparent displacement  $\mathbf{u}(x)$  that gives the point  $x'$  at time 2. Let us compute the length variation through time of the couple of points  $(x, x + \delta x)$  which are very close.

$$\begin{aligned} \delta x' &= \delta x + \mathbf{u}(x + \delta x) - \mathbf{u}(x) = \delta x + \nabla \mathbf{u} \cdot \delta x + o(\|\delta x\|^2) \quad (\text{As we assume } \delta x \text{ small}) \\ \delta x' &\simeq (Id + \nabla \mathbf{u}) \cdot \delta x = (\nabla \phi) \cdot \delta x \quad (\text{In a first order approximation}) \end{aligned}$$

This result allows to compute the local volume variation around the point  $x$  by:

$$\delta V' = \det[\delta x', \delta y', \delta z'] \simeq \det[\nabla \phi \cdot \delta x, \nabla \phi \cdot \delta y, \nabla \phi \cdot \delta z] = \det[\nabla \phi] \cdot \det[\delta x, \delta y, \delta z]$$

$$\boxed{\delta V' \simeq Jac_p(\phi) \cdot \delta V}$$

Thus, the evolution  $\frac{\delta V'}{\delta V}$  of a small volume in time is given by the Jacobian of the deformation function  $\phi$ . When  $Jac_p(\phi) > 1$  there is a local expansion at point P, and when  $Jac_p(\phi) < 1$  there is a local shrinking at point P.

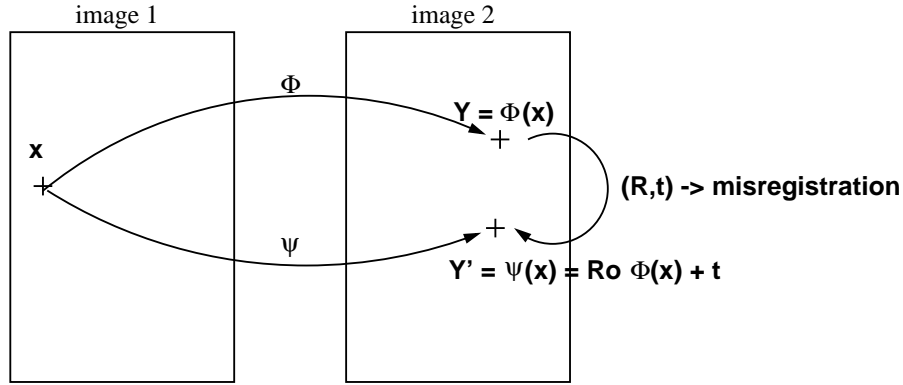


Figure 10:  $\phi$  is the deformation function for a perfect rigid registration, and  $\psi$  is the deformation function when there is a misregistration  $(R, t)$ . We have  $\psi = R \circ \phi + t$ .

### 3.2.2 Robustness of the Jacobian with respect to misalignment

Figure 10 shows what happens when two images are not perfectly aligned: the deformation function  $\psi$ , which is measured, is different from the theoretical one  $\phi$ . The misregistration is given by a residual rotation  $R$  and translation  $t$ . We have  $\psi = R \circ \phi + t$ .

Then we have:

$$Jac(\psi) = det(\nabla\psi) = det(\nabla(R \circ \phi + t)) = det(R \cdot \nabla\phi) = Jac(\phi)$$

Therefore the Jacobian of the theoretical deformation function (for a perfect rigid registration) is equal to the Jacobian of a measured deformation function (whatever the misregistration). Of course this requires that, even in the case of an approximate alignment of images, the non-rigid registration still computes a correct displacement field. In our case the rigid registration is performed because the non-rigid registration algorithm we use needs a good initial alignment to give a good result. Nevertheless, the rigid registration does not have to be as accurate as for the subtraction method where a better or equal to one voxel precision is required.

### 3.2.3 Computation and application of the Jacobian

We have seen that the computation of the Jacobian of the deformation  $\phi$  can be performed directly with the displacement field  $\mathbf{u}$ . We need to compute the first 9 derivatives of the displacement field  $\mathbf{u}$ :  $\frac{\partial u_x}{\partial x}, \frac{\partial u_x}{\partial y}, \frac{\partial u_x}{\partial z}, \dots, \frac{\partial u_z}{\partial z}$ . For a faster computation we use recursive filtering that gives an image for each derivative. Then, we need to store in memory the 9 derivatives to compute the Jacobian and for an image of  $256 \times 256 \times 180$  this requires about 425M-bytes of memory. So to avoid overfilling the memory space we compute the Jacobian on sub-images and then we fuse the different sub-results which include an overlapping border to avoid side effects.

The Jacobian gives a contrasted image with respect to the evolution amplitude. The more contrasted areas tend to correspond to shrinking or growing lesions. In Figure 11 we see that an important shrinking of a lesion between two images gives a dark region in the Jacobian image. On other areas, the value is almost constant and very close to 1, which indicates no apparent variation of volume. A zoom around a lesion shows that darker areas correspond to shrinking lesions.

## 3.3 Other operators

Calmon and Thirion have developed another vector field operator based on the divergence and the norm of the displacement field  $\mathbf{u}$  [TC97a] [TPS97]:

$$norm \cdot div(P) = \|\mathbf{u}(P)\| div \mathbf{u}(P) = \|\mathbf{u}(P)\| \left( \frac{\partial u_1}{\partial x} + \frac{\partial u_2}{\partial y} + \frac{\partial u_3}{\partial z} \right)$$

This operator has no simple physical meaning even if the sign of the operator gives an information about shrinking (negative values) or expansion (positive values). As we have no physical interpretation of the value, it is difficult to automatically threshold the image to extract the regions of interest.

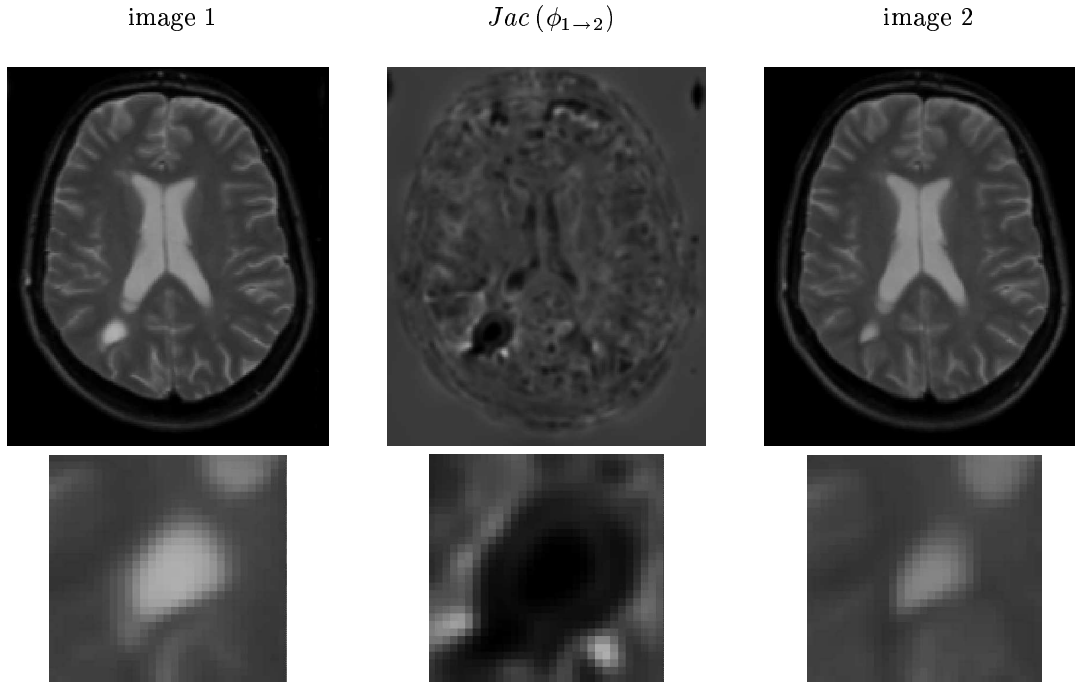


Figure 11: *Application of the Jacobian: we can see a lesion that shrinks.*

Prima et al. proposed another operator which gives the local variation of volume [PTSR98]. A cell of voxels of volume is  $V_1$  is deformed to a complex polyhedron which volume  $V_2$  is computed. Then  $\frac{V_2 - V_1}{V_1}$  is calculated. Note that another algorithm to compute  $V_2$  is given in [CRET98]. This operator is directly related to the Jacobian:

$$\frac{V_2 - V_1}{V_1} = \frac{V_2}{V_1} - 1 \simeq Jac - 1$$

Figure 12 shows the application of these three operators on the same displacement field. In particular we can notice how the Jacobian and the discrete computation of the relative variation of volume are similar. The advantage of our approach is that it provides a continuous framework for a computation (at any scale) of the Jacobian.

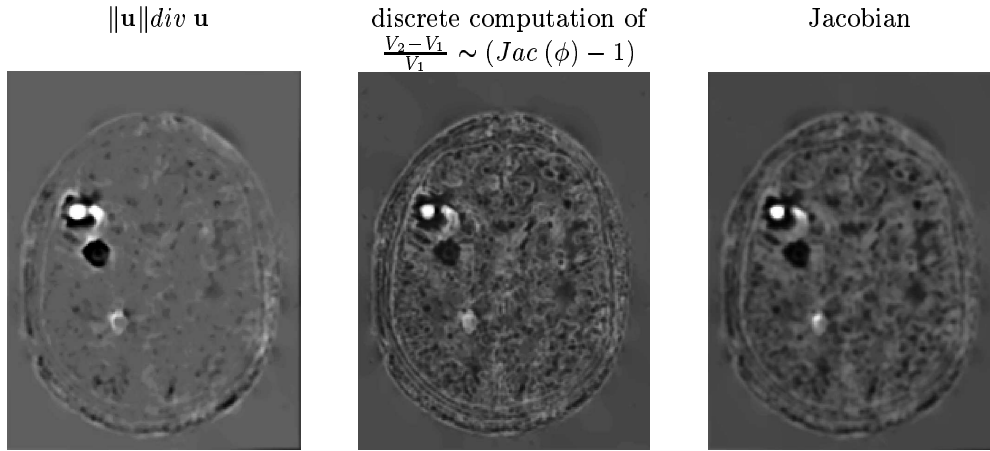


Figure 12: *Comparison between different existing operators*

## 4 Thresholding and segmentation

### 4.1 Method and results

We can extract the areas that correspond to a significant time evolution. It is possible to find a uniform threshold over the whole Jacobian image relying on its physical interpretation in terms of local variation of volume. We chose an empiric threshold of 0.3 for significant shrinking. An example in Figure 13 shows that it gives a good segmentation of a shrinking lesion.

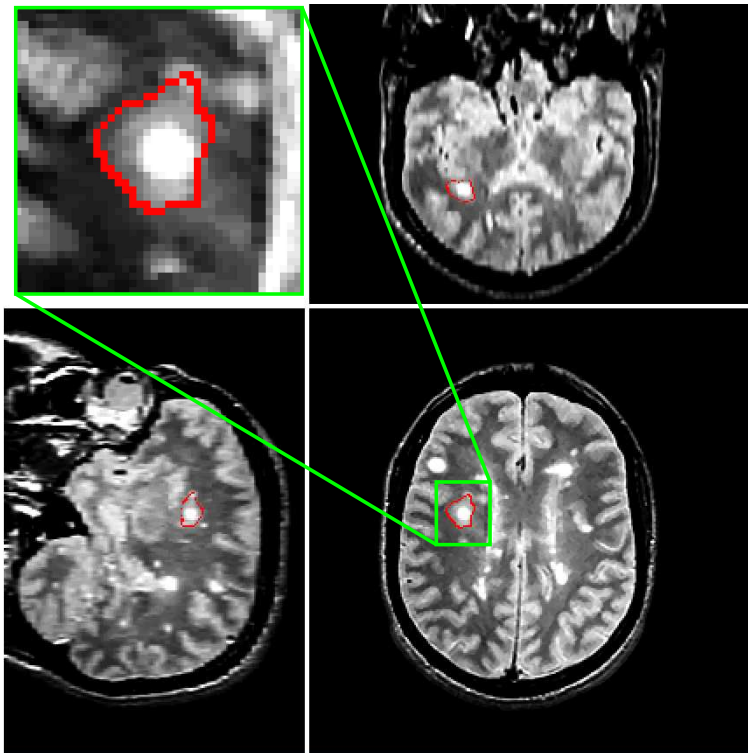


Figure 13: *The threshold  $\det(\nabla\phi) < 0.3$  makes it possible to segment shrinking lesions.*

In fact, we are going to focus only on the shrinking areas. We can see in Figure 14 that a better description is provided with the shrinking field. If there is an important expansion locally between images 1 and 2, we would need a one to many mapping due to limited resolution of the image. To avoid this, we consider only shrinking regions from 1 to 2, and then shrinking regions from 2 to 1. By thresholding shrinking areas we obtain the segmentations  $s_{1 \rightarrow 2}$  in the first image, and  $s_{2 \rightarrow 1}$  in the second image. Then we have to recombine those two information: the whole segmentations in image 1 and 2 are given by  $S_{12}(t1) = [s_{1 \rightarrow 2}] \cup [u_{2 \rightarrow 1}(s_{2 \rightarrow 1})]$ , and  $S_{12}(t2) = [s_{2 \rightarrow 1}] \cup [u_{1 \rightarrow 2}(s_{1 \rightarrow 2})]$

Figure 15 shows a shrinking lesion and a growing lesion with the corresponding displacement field and Figures 16 and 17 show automatic segmentation results obtained at two times.

### 4.2 Time series segmentation

In Figure 18, we show that with the fields between images 1 and 2 and between images 2 and 3, we can compute segmentations  $S_{12}$  in the images 1 and 2 and  $S_{23}$  in the images 2 and 3. Then we propagate the segmentations  $S_{12}$  and  $S_{23}$  respectively to times  $t3$  and  $t1$ , thanks to the vector fields  $u_{21}$  and  $u_{23}$ . Then by addition, we obtain a segmentation of the lesions in all the images of a series. In Figure 19, we can see the segmentations of lesions at three times.

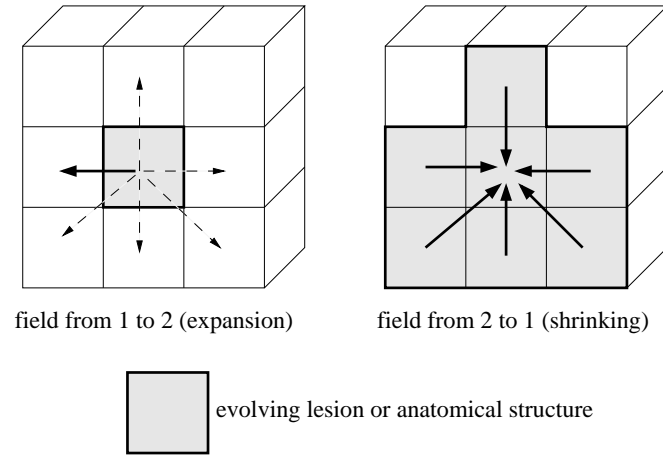


Figure 14: *The information is richer when we look at the shrinking field. Left: If there is a large expansion, the direct displacement field cannot express that one voxel should deform to several voxels. We would need a one to many mapping due to limited resolution of the image. Right: Thanks to the reverse field, a better description of the phenomenon is possible.*

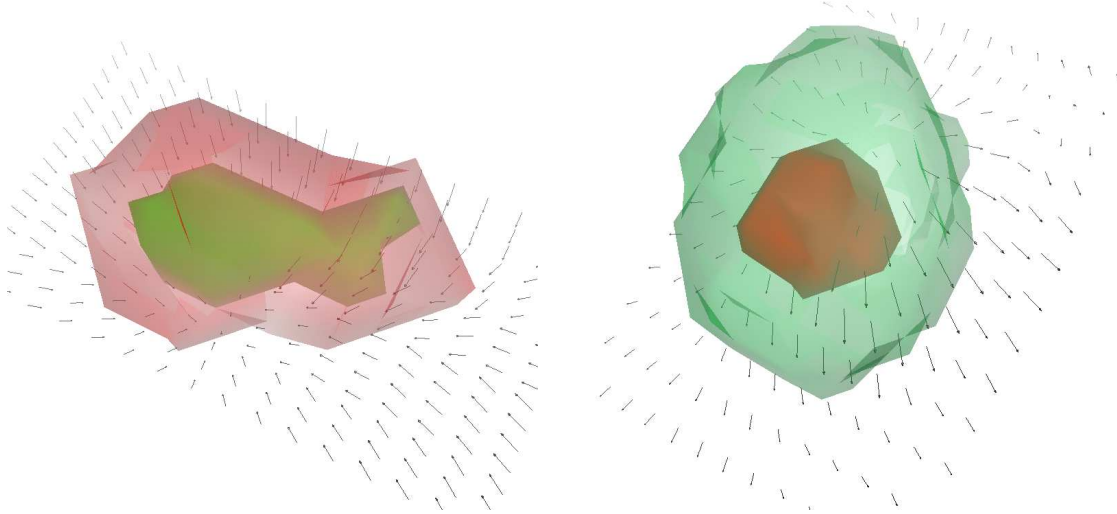


Figure 15: *Local results of evolving lesion segmentations with the vector field. Left: a shrinking lesion. Right: a growing lesion.*

## 5 Robustness with respect to rigid alignment

To study the robustness with respect to the rigid alignment, we have considered two registered images and we have shifted the second one, with a 1 degree rotation centered on the middle of the image and then with a translation of  $(1, 1, 0)$ . We can compare the results obtained by subtraction (Figure 20 top) and with our method (Figure 20 bottom) that remains stable.

## 6 Conclusion

In this report we proposed a new method to study multiple sclerosis lesions evolution through time based on the apparent displacement field between images. Thanks to the Jacobian operator we can find the significant evolving areas of images and we are able to segment the evolving lesions. This method is robust with respect to the rigid alignment. We are currently applying our approach to whole time series and we should be able to



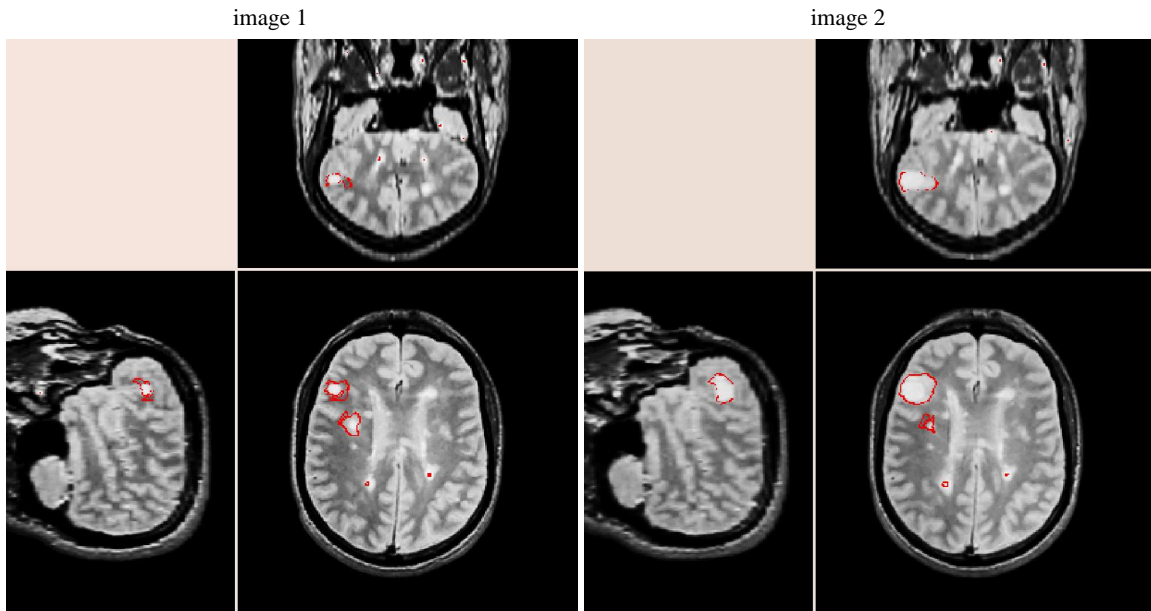


Figure 16: *Segmentation of evolving lesions (Brigham & Women's Hospital data).*

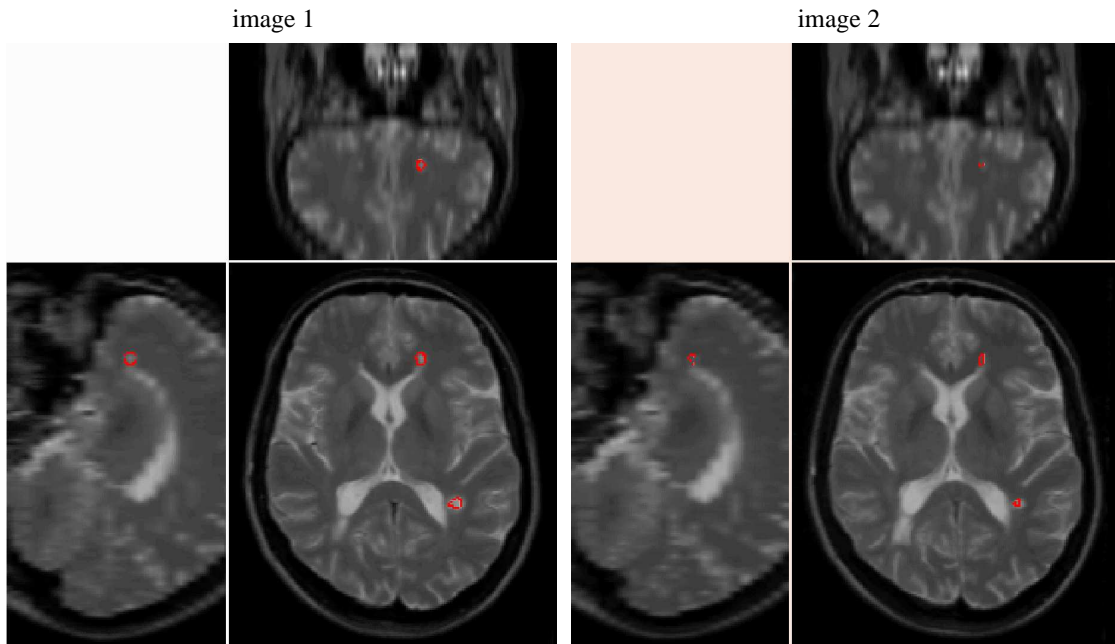


Figure 17: *Segmentation of evolving lesions (BIOMORPH data).*

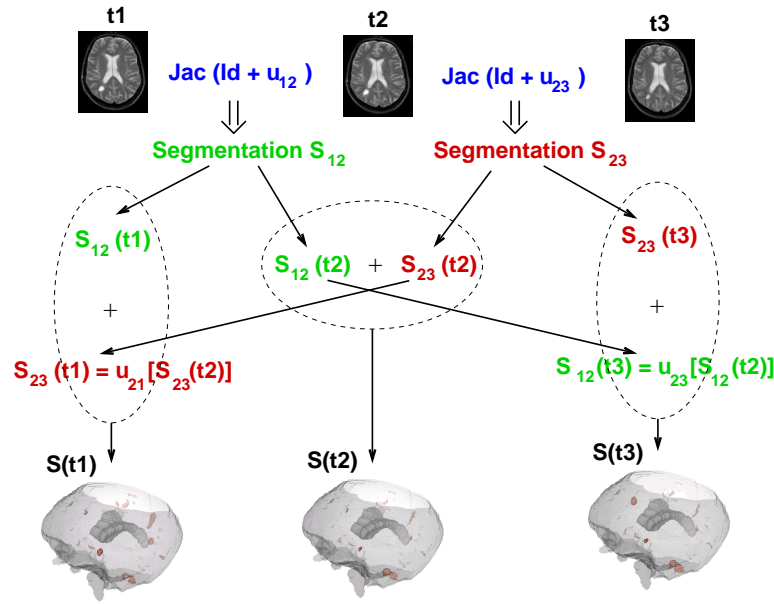


Figure 18: *Method to have time series segmentations.*

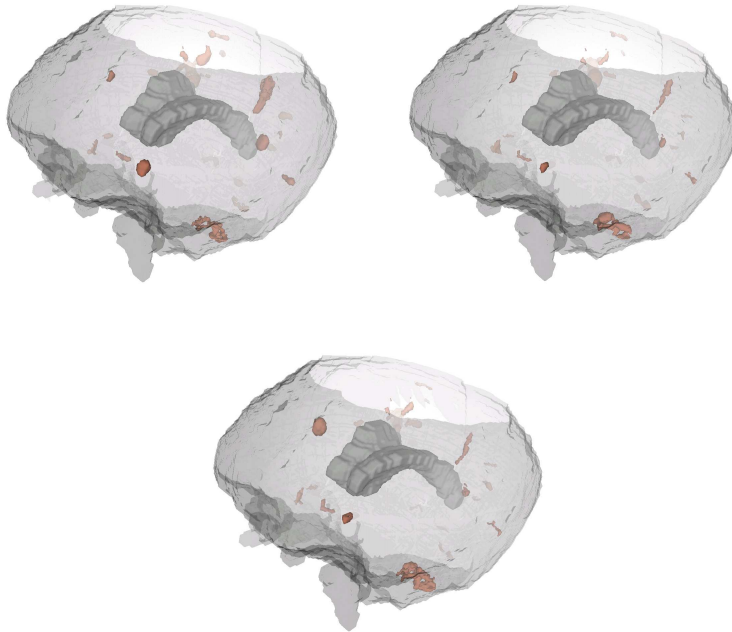


Figure 19: *Thanks to the segmentation of the evolutions between times 1 and 2, and between times 2 and 3, it is possible to visualize the lesions evolution between the 3 successive acquisitions.*

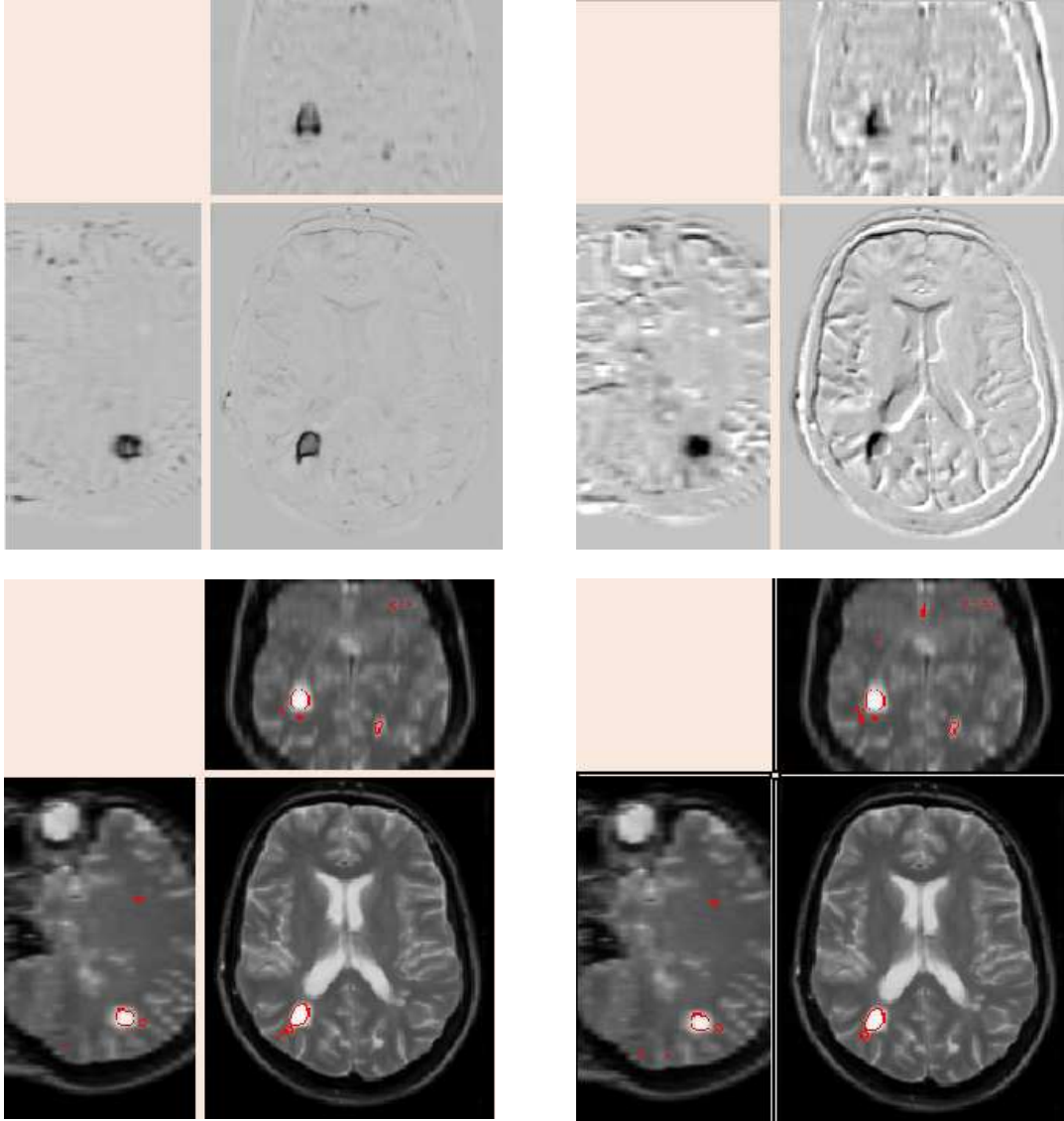


Figure 20: *Left: results with a good rigid registration (top: the subtraction; bottom: the automatic segmentation). Right: results with a misalignment (top: the subtraction; bottom: the automatic segmentation). We can see that the subtraction is very hard to study when there is a misalignment, and that the study of the vector field with the Jacobian operator is robust with respect to the rigid alignment.*

show such results very soon. Then we will compare our results with manual and other automatic segmentations [BC98]. This will be done within the BIOMORPH project. We also plan to apply our approach to study the “mass effect” by quantifying the evolution of anatomical structures such as the cerebral ventricles or the interface between grey matter and white matter.

## Acknowledgment

This work was supported by the EC-funded BIOMORPH project 95-0845, a collaboration between the Universities of Kent and Oxford (UK), ETH Zürich (Switzerland), INRIA Sophia Antipolis (France) and KU Leven (Belgium). Many thanks to Alan Colchester and Fernando Bello (University of Kent at Canterbury) for long discussions about multiple sclerosis and lesions segmentation.

We would like to thank to Charles Guttmann and Ron Kikinis, Brigham and Women’s Hospital, and Harvard Medical School, who provided us with multiple sclerosis images time series.

We warmly thank Hélène Rastouil for proofreading this report.

## References

- [BC98] F. Bello and A. Colchester. Measuring Global and Local Spatial Correspondence Using Information Theory. In W.M. Wells, A. Colchester, and S. Delp, editors, *the First International Conference on Medical Image Computing and Computer-Assisted Intervention, MICCAI'98*, volume 1496 of *Lecture Notes in Computer Science*, pages 964–973, Boston, USA, October 1998.
- [BN97] M. Bro-Nielsen. *Medical Image Registration and Surgery Simulation*. PhD thesis, IMM, July 1997. Electronic version: <http://www.imm.dtu.dk/documents/users/bro/phd.html>.
- [CRET98] G. Calmon, N. Roberts, P. Eldridge, and J. P. Thirion. Automatic Quantification of Changes in the Volume of Brain Structures. In W.M. Wells, A. Colchester, and S. Delp, editors, *the First International Conference on Medical Image Computing and Computer-Assisted Intervention, MICCAI'98*, volume 1496 of *Lecture Notes in Computer Science*, pages 964–973, Boston, USA, October 1998.
- [DVR<sup>+</sup>96] C. Davatzikos, M. Vaillant, S. Resnick, J.L. Prince, S. Letovsky, and R.N. Bryan. Morphological Analysis of Brain Structures Using Spatial Normalization. In K.H. Höhne and R. Kikinis, editors, *Visualization in Biomedical Computing*, number 1131 in *Lecture Notes in Computer Science*, pages 355–360, Hamburg, Germany, September 1996. Springer. Electronic version : [http://iacl.ece.jhu.edu/prince/jlp\\_pubs.html](http://iacl.ece.jhu.edu/prince/jlp_pubs.html).
- [GWG<sup>+</sup>98] G. Gerig, D. Welte, C. Guttman, A. Colchester, and G. Székely. Exploring the Discrimination Power of the Time Domain for Segmentation and Characterization of Lesions in Serial MR Data. In W.M. Wells, A. Colchester, and S. Delp, editors, *the First International Conference on Medical Image Computing and Computer-Assisted Intervention, MICCAI'98*, volume 1496 of *Lecture Notes in Computer Science*, pages 469–480, Boston, USA, October 1998.
- [HSO<sup>+</sup>95] J. V. Hajnal, N. Saeed, A. Oatridge, E. J. Williams, I. R. Young, and G. Bydder. Detection of Subtle Brain Changes Using Subvoxel Registration and Subtraction of Serial MR Images. *Journal of Computer Assisted Tomography*, 19(5):677–691, September 1995.
- [Lem97] L. Lemieux. The Segmentation and Estimation of Noise in Difference Images of Co-registered MRI Scan Pairs. In *Medical Image Understanding and Analysis (MIUA'97)*, Oxford, UK, Oxford, UK, July 1997. Electronic version : [http://www.robots.ox.ac.uk/mvl/frame\\_proceedings.html#Registration](http://www.robots.ox.ac.uk/mvl/frame_proceedings.html#Registration).
- [PT97] X. Pennec and J.P. Thirion. A Framework for Uncertainty and Validation of 3D Registration Methods based on Points and Frames. *IJCV*, 25(3):203–229, 1997. Electronic version: <http://www.inria.fr/epidaure/personnel/pennec/Publications.html>.
- [PTSR98] S. Prima, J.-P. Thirion, G. Subsol, and N. Roberts. Automatic Analysis of Normal Brain Dissymmetry of Males and Females in MR Images. In W.M. Wells, A. Colchester, and S. Delp, editors, *the First International Conference on Medical Image Computing and Computer-Assisted Intervention, MICCAI'98*, volume 1496 of *Lecture Notes in Computer Science*, pages 770–779, Boston, USA, October 1998.
- [TC97a] J.P. Thirion and G. Calmon. Deformation Analysis to Detect and Quantify Active Lesions in 3D Medical Image Sequences. Technical Report 3101, INRIA, February 1997. Electronic version: <http://www.inria.fr/RRRT/RR-3101.html>.
- [TC97b] J.P. Thirion and G. Calmon. Measuring Lesion Growth from 3D Medical Images. In *IEEE Non-rigid and Articulated Motion Workshop (NAN'97)*, Puerto Rico, June 1997. Electronic version: <http://www.inria.fr/RRRT/RR-3101.html>.
- [Thi96] J. Ph. Thirion. New Feature Points Based on Geometric Invariants for 3D Image Registration. *International Journal of Computer Vision*, 18(2):121–137, May 1996. Electronic version: <http://www.inria.fr/RRRT/RR-1901.html>.
- [Thi98] J.P. Thirion. Image matching as a diffusion process: an analogy with Maxwell's demons. *Medical Image Analysis*, 2(3):243–260, 1998. Electronic version: <http://www.inria.fr/RRRT/RR-2547.html>.

- [TPS97] J.P. Thirion, S. Prima, and G. Subsol. Statistical Analysis of Dissymmetry in Volumetric Medical Images. Technical Report 3178, INRIA, June 1997. Electronic version: <http://www.inria.fr/RRRT/RR-3178.html>.
- [WMG97] J.A. Weiss, B.N. Maker, and S. Govindjee. Finite Element Implementation of Incompressible, Transversely Isotropic Hyperelasticity. *Computer Methods in Applied Mechanics and Engineering*, (135):107–128, January 1997.
- [ZFE98] A. Zijdenbos, R. Forghani, and A. Evans. Automatic Quantification of MS Lesions in 3D MRI Brain Data Sets: Validation of INSECT. In W.M. Wells, A. Colchester, and S. Delp, editors, *the First International Conference on Medical Image Computing and Computer-Assisted Intervention, MICCAI'98*, volume 1496 of *Lecture Notes in Computer Science*, pages 439–448, Boston, USA, October 1998.



---

Unité de recherche INRIA Sophia Antipolis  
2004, route des Lucioles - B.P. 93 - 06902 Sophia Antipolis Cedex (France)

Unité de recherche INRIA Lorraine : Technopôle de Nancy-Brabois - Campus scientifique  
615, rue du Jardin Botanique - B.P. 101 - 54602 Villers lès Nancy Cedex (France)

Unité de recherche INRIA Rennes : IRISA, Campus universitaire de Beaulieu - 35042 Rennes Cedex (France)

Unité de recherche INRIA Rhône-Alpes : 655, avenue de l'Europe - 38330 Montbonnot St Martin (France)

Unité de recherche INRIA Rocquencourt : Domaine de Voluceau - Rocquencourt - B.P. 105 - 78153 Le Chesnay Cedex (France)

---

Éditeur  
INRIA - Domaine de Voluceau - Rocquencourt, B.P. 105 - 78153 Le Chesnay Cedex (France)  
<http://www.inria.fr>  
ISSN 0249-6399